J Mater Sci (2018) 53:538–548

Chemical routes to materials

One-pot synthesis of graphene quantum dots–phthalocyanines supramolecular hybrid and the investigation of their photophysical properties

Gertrude Fomo[1,*], Ojodomo J. Achadu[1], and Tebello Nyokong[1]

[1] *Rhodes/DST Centre for Nanotechnology Innovation, Department of Chemistry, Rhodes University, Grahamstown 6140, South Africa*

Received: 3 July 2017
Accepted: 30 August 2017
Published online: 5 September 2017

ABSTRACT

The synthesis of graphene quantum dots (GQDs) using organic compounds as carbon sources via bottom-up approaches has been widely developed, whereas their hybrids with other materials have been previously achieved post-synthetically via multi-step procedures. A novel approach for the preparation of supramolecular hybrid conjugates of GQDs and phthalocyanines (Pcs) via an in situ one-step bottom-up route was employed in this study. The as-synthesized GQDs and their Pc conjugates were characterized using different spectroscopic techniques and their photophysicochemical properties evaluated. Notably, the singlet oxygen quantum yields of the Pcs in the presence of GQDs were found to be 0.51 and 0.74 for **1**-GQDs and **2**-GQDs, respectively, as compared to the Pcs alone (0.18 and 0.70 for complex **1** and **2,** respectively). The increase in triplet quantum yield (Φ_T) values is complemented by a decrease in fluorescence quantum yield (Φ_F). Φ_T value of 0.96 obtained for the complex **2** after conjugation with GQDs is better or higher than the value of 0.74 as reported in the literature when complex **2** was conjugated to semiconductor QDs. Hence, this novel approach resulted in the derivation of hybrid materials with potentials for various photophysicochemical applications such as photodynamic therapy and photocatalysis.

Introduction

The drive for functional materials with excellent optical and electronic properties is been pushed toward carbon-based nanomaterials and their supramolecular hybrids with organic molecules and macrocycles such as phthalocyanines (Pcs), porphyrins (Ps), and spiropyrans, due to their unique chemical and physical properties [1–4]. Recent advances in nanomaterials and their syntheses have recorded a boost due to the addition of carbon-based quantum dots into the family of carbon-nanomaterials. Carbon-based nanomaterials such as graphene

Address correspondence to E-mail: fomogertrude@gmail.com

DOI 10.1007/s10853-017-1539-y

quantum dots (GQDs) exhibit excellent optical properties [5, 6], they are known to be non-toxic, biocompatible, highly water soluble, and photostable compared to the conventional semiconductor quantum dots [7]. GQDs are good energy and/or electron donors when linked with acceptor molecules (such as porphyrins and phthalocyanines) [8–10]. Due to their synthetic versatility and wide array of precursor materials, there is on-going interest in the applications of GQDs in many areas such as in biological labeling, optoelectronics, sensing, photodynamic therapy (PDT), and photocatalysis [11–13].

On the other hand, phthalocyanines (Pcs) are versatile functional macrocycles that have attracted a great deal of interests because they exhibit excellent photophysical properties [14, 15]. Pcs have been largely employed as functional materials in various photophysicochemical processes, which essentially include photodynamic therapy (PDT) and photovoltaics due to their propensities to act as efficient photosensitizers [1–3, 14, 15]. For efficient photosensitization, high triplet quantum yields and long lifetimes are required, and may be achieved by the insertion of metals such as zinc, aluminum, or silicon into Pcs rings or by conjugating them with quantum dots [16, 17]. Recently, nanoconjugates of GQDs and Pcs or Ps were reported for sensing and photocatalysis applications [9, 10]. The hybrids containing GQDs and Pcs were reportedly prepared via multistep procedures involving covalent and non-covalent (π–π stacking) interactions. However, no reports exist where supramolecular hybrids of GQDs and macrocycles (such as Pcs and Ps) have been prepared via a one-step approach, hence the focus of this work by synthesizing GQDs-Pcs supramolecular hybrids via in situ one-step process. Further, the photophysicochemical properties of the supramolecular hybrids were investigated. Fluorinated Pcs (Complex **1** and **2**, Scheme 1) were employed as model Pcs for the in situ grafting to GQDs since they have been reported to show improved photophysical and photochemical activity alone [16].

Pcs are known efficacious photosensitizers for PDT [18, 19]. However, poor solubility and aggregation of Pcs in aqueous media is a disadvantage for their use as photosensitizers. It is envisaged that the incorporation of Pcs (via in situ grafting) directly onto the edges or surface of GQDs would improve their solubility and further boost their singlet oxygen generation potential for photophysicochemical processes. Expectedly, the prepared supramolecular hybrids exhibited enhanced singlet oxygen generation occasioned by high triplet quantum yields and excellent solubility in aqueous medium, which are the desired properties of potential photosensitizers for various photophysicochemical applications.

Experimental section

Materials

N,N-dimethyl formamide (DMF) and dimethyl sulphoxide (DMSO) were purchased from Merck; ultra-pure water was obtained from a Milli–Q Water System (Millipore Corp, Bedford, MA, USA). Ascorbic acid, sodium hydroxide, 1,3-Diphenyl-2-benzofuran (DPBF) and 1,8-diazabicyclo[5.4.0] undec-7-ene (DBU) were purchased from Sigma-Aldrich. Complexes **1** and **2** were synthesized following procedures reported in the literature [16].

Equipment

Infrared spectra were collected on a Bruker Alpha model FT-IR Spectrometer with platinum ATR. Excitation and emission spectra were recorded on a Varian Eclipse spectrofluorimeter. The excitation wavelengths and slit width (each 5 nm) were kept constant for all the experiments. Ground state electronic absorption spectra were performed on a Shimadzu UV-2550 spectrophotometer in the range of 300–800 nm.

A Bruker Vertex 70-Ram II Raman spectrometer (equipped with a 1064 nm Nd:YAG laser and liquid nitrogen cooled germanium detector) was used to collect Raman data.

Triplet quantum yields were determined using a laser flash photolysis system. The excitation pulses were produced using a tunable laser system consisting of an Nd:YAG laser (355 nm, 135 mJ/4–6 ns) pumping an optical parametric oscillator (OPO, 30 mJ/3–5 ns) with a wavelength range of 420–2300 nm (NT-342B, Ekspla) as reported before [20]. The triplet lifetimes were determined by exponential fitting of the kinetic curves using the program OriginPro 7.5.

Fluorescence lifetimes were measured using a time correlated single photon counting setup (TCSPC) (FluoTime 300, Picoquant® GmbH) with a diode laser

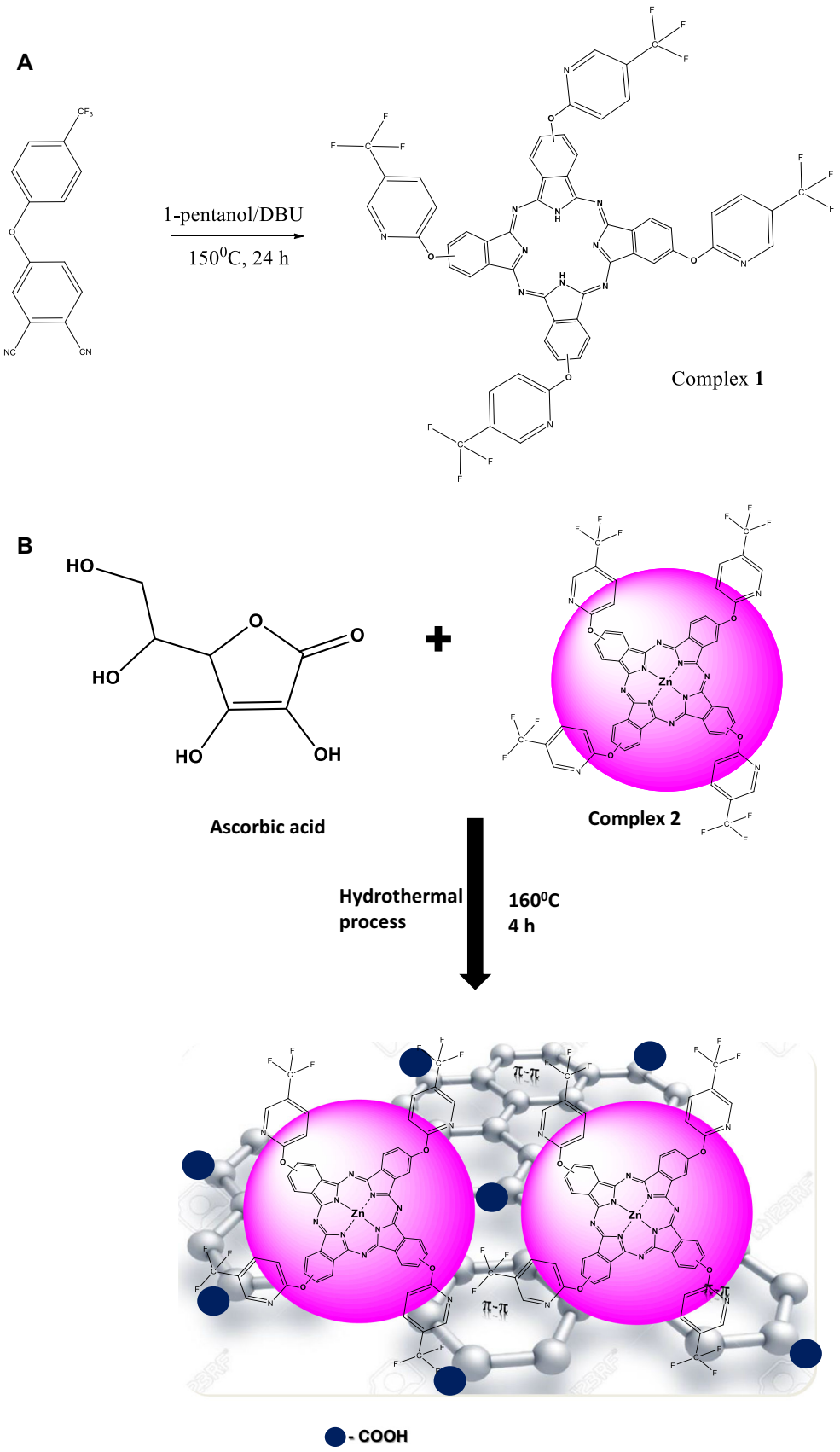

Scheme 1 Illustration of the synthesis of **a** complex **1** and **b** **2**-GQDs conjugate (as an example).

(LDH-P-485 and LDH-P-670, Picoquant® GmbH, 20 MHz repetition rate, 44 ps pulse width) as reported before [20]. LDH-P-485 was used for exciting the Pcs-GQDs conjugates at a wavelength where QDs absorb, while LDH-P-670 was used at the wavelength where Pcs absorption

X-ray photoelectron spectroscopy (XPS) analysis was done using an AXIS Ultra DLD (supplied by Kratos Analytical) using Al (monochromatic) anode equipped with a charge neutralizer, the following parameters were used: The emission was 10 mA, the anode (HT) was 15 Kv, and the operating pressure was below 5×10^{-9} Torr. A hybrid lens was used, and resolution to acquire scans was at 160 eV pass energy in slot mode. The center used for the scans was at 520 eV (width of 1205 eV) with steps at 1 eV and dwell time at 100 ms. The high-resolution scans were acquired using 80 eV pass energy in slot mode. The chemically distinct species were resolved using a nonlinear least squares curve fitting procedure. The core level binding energies (BEs) were aligned with respect to the C 1s binding energy (BE) of 284.5 eV. Dynamic light scattering (DLS) was measured using a Malvern Zetasizer Nanoseries, Nano-ZS90. Irradiation for singlet oxygen quantum yield was performed using a general electric quartz lamp (300 W) as described in the literature [21]. Light intensity was measured with a POWER MAX 5100 (Molelectron® detector incorporated) power meter and was found to be 9.27×10^{15} photons cm^{-2} s^{-1}.

Synthesis

Synthesis of 4-((5-(trifluoromethyl)pyridin-2-yl)oxy)phthalocyanine (1)

4-((5-(trifluoromethyl)pyridin-2-yl)oxy)phthalonitrile was synthesized as reported previously [16]. Complex **1** was synthesized as follows: A mixture of 4-((5-(trifluoromethyl)pyridin-2-yl)oxy)phthalonitrile (0.4 g, 1.38 mmol) and a catalytic amount of DBU in 3 mL of 1-pentanol was heated at 145 °C under nitrogen with stirring. After 24 h, the reaction mixture was cooled to room temperature, and then diluted with 15 mL methanol: Water (1:1) until the crude product precipitated. The precipitate was centrifuged and washed with the same mixture, then dried in vacuo. ^{1}H NMR (600 MHz, DMSO) δ 7.25 (t, J = 7.56 Hz, 5H), 7.20 (m, 1H), 7.12 (m, 7H), 7.04 (d, J = 15.7 Hz, 7H), 6.95 (d, J = 15.9 Hz, 4H). FT-IR: 1155 cm^{-1} (C–O stretching), 1329 cm^{-1}(C–N stretching), 1683 cm^{-1} (C=C stretching), 2934 cm^{-1} (N–H, C–H stretching). Anal. Calc. for $C_{60}H_{39}N_{11}O_4$: C, 56.75; H, 2.26; N, 12.78. Found: C, 55.81; H, 2.93; N, 13.39. MALDI TOF-MS: Calculated: 1158.86; Found: 1163.98 $[M + 5]^+$. UV/Vis (DMF) λ_{max}/nm (Log ε): 673 (4.09), 608 (3.44), 340 (3.75).

Synthesis of GQDs and their Pcs supramolecular hybrids

Ascorbic acid (0.42 g, 24.8 mmol), NaOH (0.24 g, 60.0 mmol), and complex **1** (0.02 g, 0.017 mmol) or **2** (0.02 g, 0.015 mmol) were diluted with Millipore water (10 mL) under stirring for 20 min. The reaction mixture was transferred into a Teflon-lined hydrothermal reactor and heated for 4 h at 160 °C under stirring. The obtained dark solution was filtered using 2.0 μm membrane filter to remove large particles. The dialysis membrane was activated with hot water and cleaned with Millipore water. The filtered solutions were transferred into a beaker and topped up with Millipore water and stirred for 48 h. The resulting hybrids are denoted as **1**-GQDs and **2**-GQDs. GQDs alone were synthesized using the same precursors and procedures described above without the Pcs.

Photophysicochemical studies

Fluorescence (Φ_F), triplet (Φ_T), and singlet oxygen (Φ_Δ) quantum yields

Fluorescence (Φ_F), triplet (Φ_T), and singlet oxygen (Φ_Δ) quantum yields were determined in DMF using comparative method described in the literature [17, 22]. Unsubstituted ZnPc was used as a standard ($\Phi_F = 0.20$ in DMSO [22]), ($\Phi_T = 0.58$ in DMF [17]), and $\Phi_\Delta = 0{:}56$ in DMF [17].

The quenching efficiency of the triplet-excited state by singlet oxygen is given by S_Δ, Eq. 1 [22].

$$S_\Delta = \frac{\Phi_\Delta}{\Phi_T} \quad (1)$$

Förster resonance energy transfer (FRET) parameters

Förster resonance energy transfer (FRET) is a non-radiative energy transfer from a photoexcited donor fluorophore to an acceptor molecule. FRET is dependent on many parameters such as the center-to-

center separation distance between donor and acceptor (r) and the spectral overlap between the donor emission and acceptor absorption spectrum (J) [23]. FRET efficiency (Eff) was determined from the steady-state and/or time-resolved fluorescence measurements, using Eq. 2 [24]:

$$\mathrm{Eff} = 1 - \frac{\Phi^{\mathrm{con}}_{\mathrm{F(GQDs)}}}{\Phi_{\mathrm{F(GQDs)}}} \quad (2)$$

where $\Phi_{\mathrm{F(GQDs)}}$ and $\Phi^{\mathrm{con}}_{\mathrm{F(GQDs)}}$ are the donor's fluorescence intensity in the absence and presence of the acceptor, respectively. FRET process results in the loss of the donor's fluorescence coupled with an enhancement of the acceptor's fluorescence signal if the latter is an emitter. Similarly, energy transfer can translate into the shortening of the excited state lifetime of the donor coupled with a lengthening of the acceptor's lifetime [17].

FRET efficiency (Eff) is related to the rate of energy transfer and the lifetime as shown in Eq. 3 [24].

$$\mathrm{Eff} = \frac{K_{\mathrm{D-A}}}{K_{\mathrm{D-A}} + \tau_{\mathrm{D}}^{-1}} \quad (3)$$

where τ_{D} is the lifetime of the donor in the absence of acceptor, and $K_{\mathrm{D-A}}$ is the rate of energy transfer from donor to acceptor.

Results and discussion

Synthesis and characterization of complex 1

The synthesis of complex **1** (Scheme 1) was achieved when 4-((5-(trifluoromethyl)pyridin-2-yl)oxy) phthalonitrile was condensed in 1-pentanol in the presence of DBU as a catalyst. Complex **1** was characterized using spectroscopic techniques and elemental analysis. FT-IR spectrum showed the disappearance of the C≡N peak at 2239 cm^{-1} of the precursor compound upon formation of complex **1**, this result confirmed the formation of the latter. ^{1}H NMR spectrum showed that the aromatic protons were remarkably deshielded (due to the strong electron donating fluorine groups), ranging from 6.95 to 7.25 ppm. The elemental analysis of complex **1** gave the expected percentages. The mass distribution spectrum of complex **1** had molecular ion peaks at m/z 1158.86; $[M]^+$ and 1163.98 $[M + 5]^+$. Fragmentation of Pcs molecular ion peaks into $[M]^+$, $[M + nH]^+$, or $[M - nH]^-$ have been reported [25], hence the observed mass spectra pattern for complex **1**.

Characterization of 1-GQDs and 2-GQDs

TEM and DLS

TEM images of GQDs and their hybrid conjugates are as shown in Fig. 1A (a, b). The GQDs are monodispersed, whereas the conjugates showed a clustering of the GQDs nanoparticles in the presence of the Pcs due to the aggregation tendencies of Pcs [26]. Figure 2b shows the DLS plots for GQDs alone and **1**-GQDs conjugate (as an example) with sizes of about 6.5 and 33 nm, respectively, which shows an increase in the size of GQDs upon coordination to the Pcs.

FT-IR, Raman and XRD analysis

Figure 2 shows the comparative FT-IR spectra of complex **1**, GQDs, and **1**-GQDs, respectively. The bands observed at 1115 cm^{-1} (for complex **1**) and 1061 cm^{-1} (for **1**-GQDs) correspond to C-O stretching vibrations. The vibrational band around 1570 cm^{-1} corresponds to C=O of the surface carboxylic group on the GQDs. The peak at 1326 cm^{-1} (for complex **1**), 1319 cm^{-1} (for **1**-GQDs) could be attributed to the C–

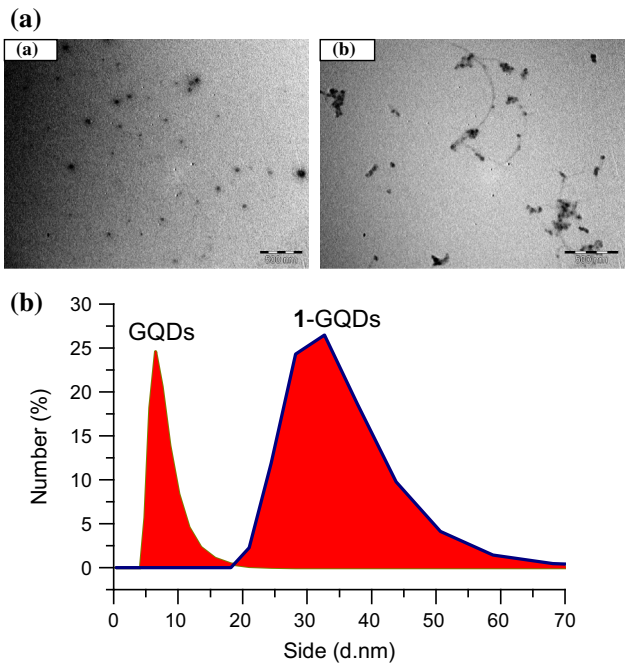

Figure 1 **A** TEM images of GQDs **a** and 1-GQDs conjugate and **B** Size of GQD and **1**-GQDs conjugate determined using DLS.

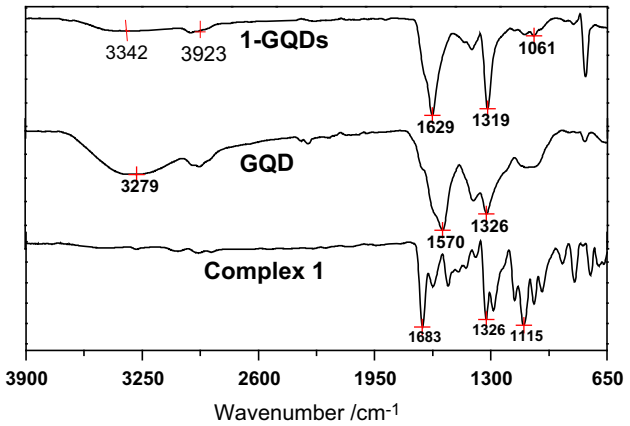

Figure 2 FT-IR of complex **1**, GQDs and **1**-GQDs.

N stretching of the Pc complex. The peaks around 1500–1600 cm^{-1} corresponds to C=C stretching vibrations within the respective complexes and GQDs. By comparing the FT-IR spectra of **1**-GQDs hybrid with that of complex **1** and GQDs alone, there are indications of new complex formation. This observation indicates the likely conjugation of the Pcs to GQDs.

Figure 3a displays the Raman spectra of the GQDs and their hybrid conjugates. The characteristic G and D bands were observed at around 1560 and 1360 cm^{-1}, respectively, for the GQDs [27]. The hybrid conjugates of the GQDs and Pcs exhibited some shifts in the D and G bands, showing the formation of new nanocomplexes. The increase in D band could be due to the disorder created by the Pcs within the GQDs layers [28]. The I_D/I_G ratios of 0.10 and 0.36 were obtained for GQD and **1**-GQDs, respectively. Thus, there is an increase in the I_D/I_G ratio for **1**-GQDs which indicates the introduction of defects on the GQDs nanostructure in the presence of the Pcs.

Structural characterization of the supramolecular hybrids was further carried out using powder XRD, and the patterns are shown in Fig. 3b. XRD pattern of the GQDs alone exhibits a main (broad) diffraction peak at $2\Theta = 19°$ which is due to (002) Bragg's reflection of the carbon in the graphene layers [5, 29]. The broadness of the XRD peak for the GQDs reflects their small size [29]. The XRD of **2**-GQDs conjugate with a broad peak at $2\Theta = 27°$ with sharp peaks embedded at $2\Theta = 11°$ and $\sim 50°$ is typical of hybrid conjugates of carbon-nanomaterials and Pcs as reported previously [11, 30]. The broadened and/or shifts in the XRD patterns of the hybrid conjugate

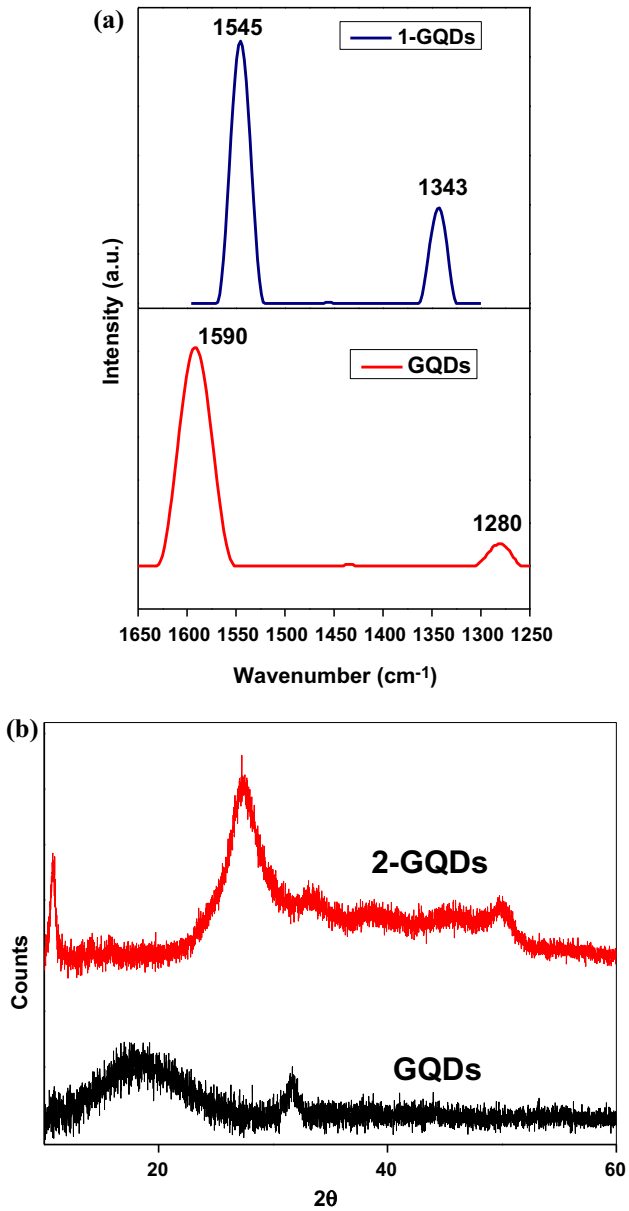

Figure 3 **a** Raman spectra of GQDs and **1**-GQDs and **b** XRD pattern of GQDs and their hybrid conjugate (shown as an example).

may signify interactions between the GQDs and Pcs and could thus indicate the formation of new complexes between the GQDs and the respective Pcs.

X-ray photoemission spectroscopy (XPS)

XPS was employed to characterize the as-synthesized conjugates to confirm the bonding states of the GQDs and hybrid conjugates (using **1**-GQDs as an example). The XPS survey spectra, Fig. 4a, of the GQDs

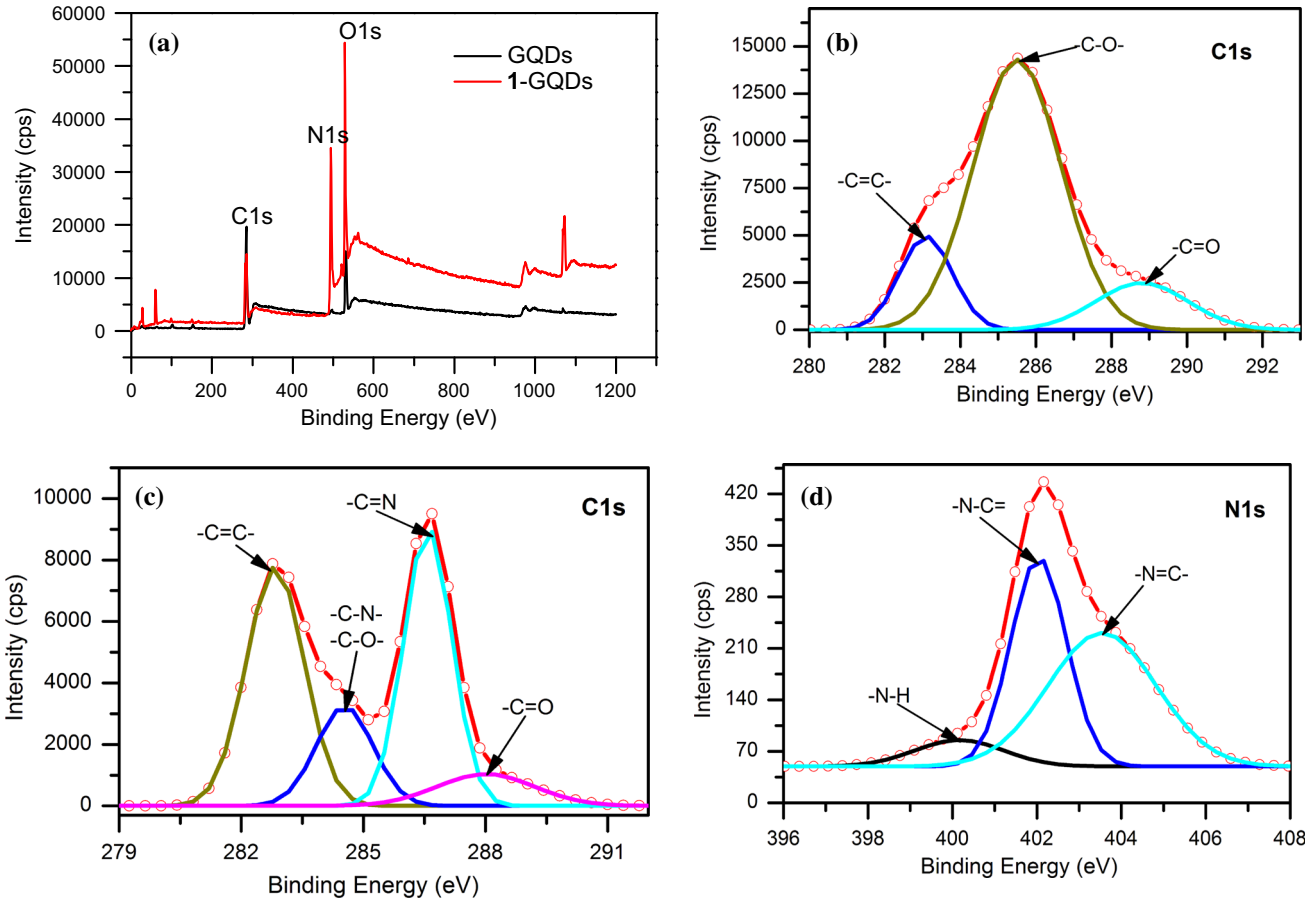

Figure 4 **a** Wide scan, **b** C1 s of GQDs, **c** C1 s of **1**-GQDs and **d** N1 s of **1**-GQD (as an example).

and **1**-GQDs showed a distinct graphitic peak at ca. 285 eV and at ca. 533 eV which correspond to C 1s and O 1s, respectively [31, 32]. In addition, **1**-GQDs hybrid conjugate showed an N 1s peak due to complex **1** which is absent in the spectra of GQDs alone (Fig. 4a). The high-resolution C 1s spectrum of the GQDs (Fig. 4b) indicates the existence of different bonding states of C–C and C=C (283.13 eV), C–O (285.47 eV) and C=O (288.79 eV) typical of GQDs [33]. Figure 4c shows the high-resolution C 1s of **1**-GQDs conjugate with C–C and C=C (282.75 eV), C–O (284.55 eV), C=O (288.10 eV), and –C=N (286.67 eV). The later peak (–C=N) observed in the conjugate was not found in the GQDs alone. The N 1s signal of the hybrid conjugate was further deconvoluted, and the obtained high-resolution N 1s spectrum (Fig. 4d) demonstrated the existence of –N–H (399.8 eV) and C–N (402.3 eV) (due to Pc), further indicating the successful formation of new supramolecular hybrid materials of GQDs and Pcs.

Ground state electronic absorption

The ground state absorption spectra of the Pcs and their GQDs conjugates are shown in Fig. 5. For complex **1,** the lack of split Q band observed is due to the basic solvents employed [34]. Complex **1** also shows aggregation with broadening near 630 nm. Aggregation in Pcs is due to π–π stacking interaction of the aromatic rings resulting in broad or split Q bands, with the low energy band being due to the monomer and the high energy band due to the aggregate [26]. Complex **2** and **2**-GQDs conjugate showed narrow Q bands suggesting monomeric behavior, Fig. 5. The Q band maxima for the Pcs and their GQDs conjugates are summarized in Table 1. The B band region was observed between 337 and 340 nm for the Pcs and their conjugates. There are no significant shifts in the Q band of the Pcs upon conjugation, Fig. 5 and Table 1. Additional fluorescence emission, absorption, and excitation spectra for

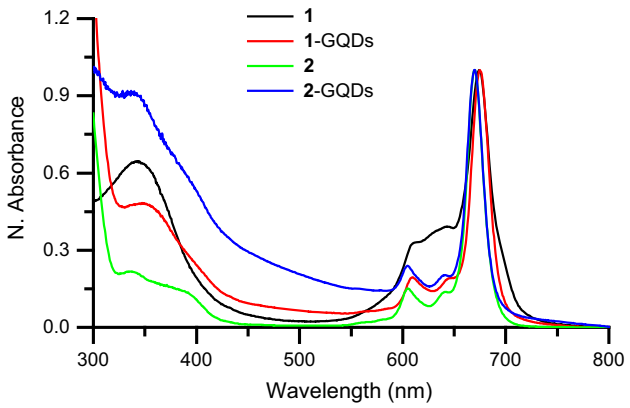

Figure 5 Absorption spectra of complex **1**, **1**-GQDs, complex **2,** and **2**-GQDs in DMF.

complex **1**, **1**-GQDs, complex **2,** and **2**-GQDs are shown in Fig. 6.

Photophysical and photochemical parameters

Fluorescence lifetime (τ_F) and quantum yield (Φ_F) studies

Figure S1 (supplementary information) shows the fluorescence decay curve of complex **1**, **1**-GQDs, complex **2,** and **2**-GQDs in DMF. The Φ_F values of the Pcs decrease after conjugation to the GQDs, Table 1. Fluorescence lifetimes (τ_F) of the conjugates are longer than that of the corresponding Pcs alone, Table 1. The observed lengthening of lifetimes for the Pcs in the presence of the GQDs may be due to the protection of the former by the latter. Upon conjugation, both the fluorescence lifetime and fluorescence quantum yield of the GQDs decreased probably due to Förster resonance energy transfer (FRET) as reportedly observed previously [11, 12] (Table 1)

FRET studies

The emission spectrum observed for complex **1** (as an example) on excitation at 360 nm presented in Figure S2 shows that in the presence of GQDs, there is an increase in emission intensity for complex **1** and a consequent decrease in the fluorescence of the GQDs. This quenching could probably be due to energy transfer from the GQDs to the Pc complexes since the absorption spectra of complexes **1** and **2** overlap with the emission spectra of the GQDs, Figure S2 (supplementary information), which is a requisite condition for FRET phenomenon [23]. The evaluated FRET parameters such as energy transfer efficiency (Eff) and rate (k_{D-A}) are shown in Table 1.

Triplet quantum yields and lifetime

Triplet quantum yield (Φ_T) is used to quantify the fraction of molecules that undergo rapid intersystem crossing from the lowest excited singlet state to populate the lowest excited triplet state. Triplet quantum yields and lifetimes (τ_T) for complex **1**, **1**-GQDs, complex **2,** and **2**-GQDs were obtained in DMF, Table 1. The Φ_T values of complexes **1** and **2** increased after conjugating with GQDs while the τ_T values of the Pcs decreased as expected. This suggests that the presence of GQDs encourages intersystem crossing from excited singlet to triplet state.

Singlet oxygen quantum yields (Φ_Δ)

A good photosensitizer must be very efficient in generating singlet oxygen, the active species of a photodynamic therapy treatment [35, 36]. Energy transfer between the triplet state of a photosensitizer (Pcs and Pcs-GQDs) and the ground state of molecular oxygen leads to the conversion of the latter into singlet oxygen. This is quantified by the singlet

Table 1 Photophysical parameters for complex **1**, **1**-GQDs, complex **2,** and **2**-GQDs in DMF at 600 nm excitation where the Pcs absorb in DMF

Compounds	λ_{abs} (nm)	Φ_F^a	τ_F (ns)[a]	Φ_Δ	Φ_T	τ_T (μs)	S_Δ	Eff	K_{D-A}
GQDs	364	(0.01)	(3.95)	–	–	–	–	–	
1	673	0.24	2.3	0.18	0.33	290	0.32	–	–
1-GQDs	674	0.22 (0.01)	4.2 (<0.01)	0.51	0.56	154	1.55	0.02	0.01
2	670	0.26	2.8	0.70	0.71	282	0.73	–	–
2-GQDs	670	0.20 (<0.01)	3.1 (3.00)	0.74	0.96	250	1.04	0.36	0.19

[a] Values in brackets are for excitation where GQDs absorb

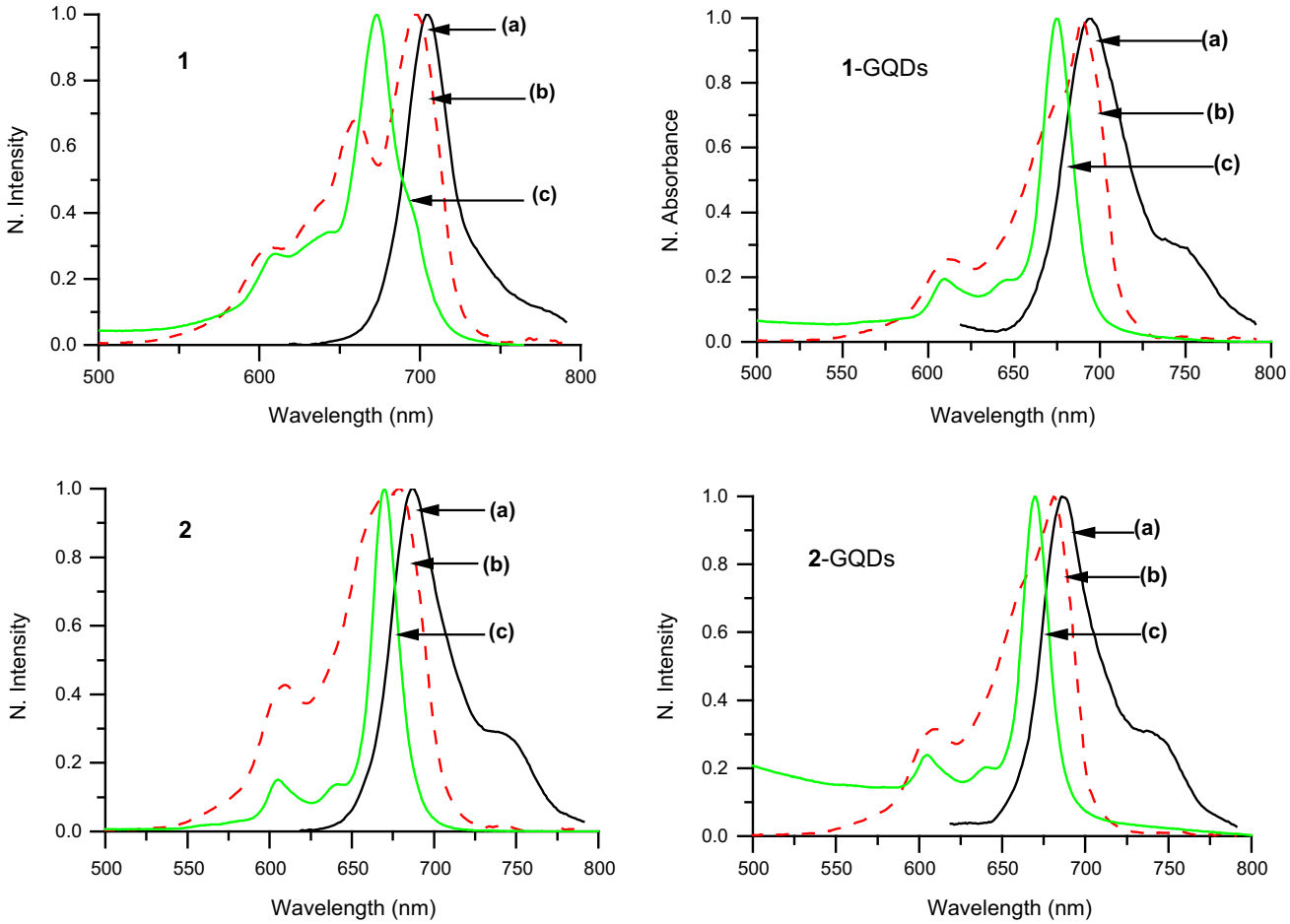

Figure 6 (*a*) Emission, (*b*) Excitation and (*c*) Absorption in DMF.

oxygen quantum yield (Φ_Δ), a parameter which gives an indication of the potential of molecules to be used as photosensitizers in applications where singlet oxygen is required. There was no decrease in the Q band and no appearance of new bands during Φ_Δ determinations (Figure S3, supplementary information), this indicates that the Pcs (**1** and **2**) were not damaged by the generated singlet oxygen. The Φ_Δ values were determined in DMF using chemical method and DPBF as a quencher and unsubstituted ZnPc as the reference. The disappearance of DPBF was monitored using UV–Vis spectrophotometer (Figure S3, supplementary information). Table 1 shows that complex **2** has a larger Φ_Δ than complex **1** due to the presence of a central metal (Zn).

Conclusion

Supramolecular hybrids of metal free (**1**) and zinc phthalocyanines (**2**) with graphene quantum dots (GQDs) were prepared by one-pot synthesis route. The as-synthesized conjugates were characterized and their photophysical properties studied. The high triplet quantum yields for the Pcs resulted in the enhanced singlet oxygen produced by the Pcs after conjugation to the GQDs. Compared to the metal free Pc, FRET mechanism (Eff) was higher for the metallated derivative (ZnPc) in the presence of the GQDs. The photophysical properties of the hybrids indicate that they are good photosensitizers for various photophysicochemical applications.

Acknowledgements

This work was supported by the African Laser Centre (ALC), the Department of Science and Technology (DST), CSIR National Laser Centre, Rental Pool Program, National Research Foundation (NRF) of South Africa through DST/NRF South African Research Chairs Initiative for Professor of Medicinal Chemistry and Nanotechnology (UID 62620), and Rhodes University.

Electronic supplementary material: The online version of this article (doi:10.1007/s10853-017-1539-y) contains supplementary material, which is available to authorized users.

References

[1] Giovanni B, De La Torre G, Torres T (2015) Phthalocyanine-nanocarbon ensembles: from discrete molecular and supramolecular systems to hybrid nanomaterials. Acc Chem Res 4:900–910

[2] Bottari G, Truhkina O, Ince M, Torres T (2012) Towards artificial photosynthesis: supramolecular, donor–acceptor, porphyrin and phthalocyanine/carbon nanostructure ensemble. Coord Chem Rev 256:2453–2477

[3] Chidawanyika W, Nyokong T (2010) Characterization of amine-functionalized single-walled carbon nanotube-low symmetry phthalocyanine conjugates. Carbon 48:2831–2838

[4] Del Canto E, Flavin K, Natali M, Perova T, Giordani S (2010) Functionalization of single-walled carbon nanotubes with optically switchable spiropyrans. Carbon 48:2815–2824

[5] Ritter AK, Lyding WJ (2009) The influence of edge structure on the electronic properties of graphene quantum dots and nanoribbons. Nat Mater 8:235–242

[6] Li Y, Shu H, Wang S, Wang J (2015) Electronic and optical properties of graphene quantum dots: the role of many-body effects. J Phys Chem 119:4983–4989

[7] Thakur K, Kumawat M, Srivastava R (2017) Multifunctional graphene quantum dots for combined photothermal and photodynamic therapy coupled with cancer cell tracking applications. RSC Adv 7:5251–5261

[8] Fan Z, Li S, Yuan F, Fan L (2015) Fluorescent graphene quantum dots for biosensing and bioimaging. RSC Adv 5:19773–19789

[9] Ge J, Lan M, Zhou B et al (2014) A graphene quantum dot photodynamic therapy agent with high singlet oxygen generation. Nat Commun 5:1–8

[10] Lu Q, Zhang Y, Liu S (2015) Graphene quantum dots enhanced photocatalytic activity of zinc porphyrin toward the degradation of methylene blue under visible-light irradiation. J Mater Chem A 3:8552–8558

[11] Achadu OJ, Uddin I, Nyokong T (2016) Fluorescence behavior of nanoconjugates of graphene quantum dots and zinc phthalocyanines. J Photochem Photobiol A Chem 317:12–25

[12] Achadu OJ, Nyokong T (2017) Graphene quantum dots coordinated to mercaptopyridine-substituted phthalocyanines: characterization and application as fluorescence "turn ON" nanoprobes. Spectrochim Acta A Mol Biomol Spectrosc 174:339–347

[13] Zhang L, Peng D, Liang RP, Qiu JD (2015) Graphene quantum dots assembled with metalloporphyrins for "Turn on" sensing of hydrogen peroxide and glucose. Chem A Eur J 21:9343–9348

[14] Nyokong T, Antunes E (2010) Photochemical and photophysical properties of metallophthalocyanines. In: Kadish KM, Smith KM, Guilard R (eds) The handbook of porphyrin science, vol 7. World Scientific, Singapore, pp 347–349

[15] Claessens CG, Hahn U, Torres T (2008) Phthalocyanines: from outstanding electronic properties to emerging applications. Chem Rec 8:75–97

[16] Erdogmus A, Moeno S, Litwinski C, Nyokong T (2010) Photophysical properties of newly synthesized fluorinated zinc phthalocyanines in the presence of CdTe quantum dots and the accompanying energy transfer processes. J Photochem Photobiol A Chem 210:200–208

[17] Wang J, Zhang Y, Ye J, Jiang Z (2016) Enhanced fluorescence of tetrasulfonated zinc phthalocyanine by graphene quantum dots and its application in molecular sensing/imaging. Luminescence 31:1–8

[18] Whitacre CM, Feyes DK, Satoh T, Grossmann J, Mulvihill JW, Mukhtar MH, Oleinick NL (2000) Photodynamic therapy with the phthalocyanine photosensitizer Pc 4 of SW480 human colon cancer xenografts in athymic mice. Clin Cancer Res 6:2021–2027

[19] Miller JD, Baron ED, Scull H, Hsia A, Berlin JC, McCormick T, Colussi V, Kenney ME, Cooper KD, Oleinick NL (2007) Photodynamic therapy with the phthalocyanine photosensitizer Pc 4: the case experience with preclinical mechanistic and early clinical–translational studies. Toxicol Appl Pharmacol 224:290–299

[20] Fashina A, Antunes E, Nyokong T (2013) Characterization and photophysical behavior of phthalocyanines when grafted onto silica nanoparticles. Polyhedron 53:278–285

[21] Ogunsipe A, Chen JY, Nyokong T (2004) Photophysical and photochemical studies of zinc(II) phthalocyanine

derivatives-effects of substituents and solvents. New J Chem 28:822–827

[22] Spiller W, Kliesch H, Wohrle D, Hackbarth S, Roder B, Schnurpfeil G (1998) Singlet oxygen quantum yields of different photo-sensitizers in polar solvents and micellar solutions. J Porphyr Phthalocyanines 2:145–158

[23] Berney C, Danuser G (2003) FRET or No FRET: a quantitative comparison. Biophys J 84:3992–4010

[24] Kossanyi J, Chahraoui D (2000) Electron transfer reaction and demetalation of phthalocyanines. Int J Photoenergy 2:9–15

[25] Tolbin AY, Pushkarev VE, Nikitin GF, Tomilova LG (2009) Heteroligand and heteronuclear clamshell-type phthalocyanines: selective preparation, spectral properties, and synthetic application. Tetrahedron Lett 69:4848–4850

[26] Stillman MJ, Nyokong T, Leznoff CC, Lever AB (1989) Phthalocyanines. Properties and application. VCH Publishers, Weinheim

[27] Ferrari AC, Robertson J (2001) Resonant Raman spectroscopy of disordered, amorphous, and diamondlike carbon. Phys Rev B 64:075414

[28] Liu L, Shen Z, Liang S, Yi M, Zhang X, Ma S (2014) Graphene for reducing bubble defects and enhancing mechanical properties of graphene/cellulose acetate composite films. J Mater Sci 49:321–328. doi:10.1007/s10853-013-7708-8

[29] Singha V, Jounga D, Zhaia L, Dasa S, Khondakera SI, Seal S (2011) Graphene based materials: past, present and future. Prog Mater Sci 56:1178–1271

[30] Yang JH, Gao Y, Zhang W, Tang P, Tan J, Lu AH, Ma D (2013) Cobalt phthalocyanine graphene oxide nanocomposite: complicated mutual electronic interaction. J Phys Chem C 117:3785–3788

[31] Zhou D, Cheng P, Luo J, Xu W, Li J, Yuan D (2017) Facile synthesis of graphene@NiMoO4 nanosheet arrays on Ni foam for a high-performance asymmetric supercapacitor. J Mater Sci 52:1–11. doi:10.1007/s10853-017-1467-x

[32] Zhang Y, Pan C (2011) TiO_2/graphene composite from thermal reaction of graphene oxide and its photocatalytic activity in visible light. J Mater Sci 46:2622–2626. doi:10.1007/s10853-010-5116-x

[33] Li Y, Zhao Y, Cheng H, Hu Y, Shi G, Dai L, Qu L (2012) Nitrogen-doped graphene quantum dots with oxygen-rich functional groups. J Am Chem Soc 134:15–18

[34] Freyer W, Mueller S, Teuchner K (2004) Photophysical properties of benzoannelated metal-free phthalocyanines. J Photochem Photobiol A Chem 163:231

[35] Darwent JR, McCubbin I, Phillips D (1982) Excited singlet and triplet state electron-transfer reactions of aluminium(III) sulphonated phthalocyanine. Chem Soc Faraday Trans 2(78):347–357

[36] Samia AC, Dayal S, Burda C (2006) Quantum dot-based energy transfer: perspectives and potential for applications in photodynamic therapy. Photochem Photobiol 82:617–625